

A Dynamic Continuous Descent Approach Methodology for Low Noise and Emission

S. Alam, M. H. Nguyen, H. A. Abbass and C. Lokan
Defence and Security Applications Research Center,
University of New South Wales
Australian Defence Force Academy, Canberra, Australia

M. Ellejmi and S. Kirby
EUROCONTROL
Cooperative Network Design (CND)
Brtigny-sur-Orge, France

Abstract—Continuous Descent Approaches (CDAs) can significantly reduce fuel burn and noise impact by keeping arriving aircraft at their cruise altitude for longer than during conventional approaches (to descend as late as possible) and then having them make a continuous descent to the runway at near idle thrust with no level flight segments. The CDA procedures are fixed routes that are vertically optimized. With the changing traffic conditions and variable noise abatement rules the benefits of CDA operations are not yet fully realized.

In this paper we propose a methodology to generate aircraft-specific dynamic CDA routes that are both laterally and vertically optimized on given objectives (noise, emission and fuel) from an Initial Approach Fix (IAF) to Final Approach Fix (FAF). The methodology utilizes real-time aircraft position and defined objectives to generate CDA routes which can then be converted into a set of artificial waypoints for continuous descent in transition airspace. The methodology involves discretizing the terminal airspace into concentric cylinders with artificial waypoints and uses enumeration and elimination (based on aircraft performance envelope) from one waypoint to other to identify all the possible routes. For each transition a variety of metrics including noise, emission and fuel burn are computed. From the resulting set of possible CDA routes, those routes are identified that represent the best trade-off on the given objectives. One of these routes is then used to dynamically update the flight route for executing the CDA procedure.

For noise we used The Overall Sound Pressure Level (OPSL) and for emissions we used four pollutants HC , CO , CO_2 and NO_x . The dynamic CDA algorithm is implemented in a high-fidelity simulator ATOMS for Sydney Terminal Area with 34L as arrival runway for a Melbourne-Sydney flight (B737-400 aircraft, CFM56-3C-1 engines with a nominal weight of 58000 kg). The dynamic CDA routes are then compared on noise, emission and fuel burn with same flight conducting a typical CDA procedure (MANFA ONE Arrival) at the Sydney airport. The results shows that the methodology generates 64 possible solutions (dynamic CDA routes) from IAF to FAF in the transition airspace, of which 5 solutions were non-dominated. Dynamic CDA approach shows a reduction of 14.96% in noise, 11.6% reduction in NO_x emission and 1.5% reduction in fuel burn when compared to a standard CDA trajectory.

The paper also investigates the throughput capacity of transition airspace for multiple flights performing CDA operation. The methodology incorporates a delay algorithm which uses the flights' estimated time of arrival (ETA) at the IAF and then allocates them a conflict free CDA route by searching through available routes. The approach takes into account the aircraft category and corresponding time occupancy at each artificial waypoint of the proposed CDA routes and propagate delays back when conflict exists.

I. INTRODUCTION

With the continued growth in air traffic, airport runways are expected to handle a higher volume of traffic [1], [2]. A consequence is that aircraft noise and local air quality becomes a concern for residents living in areas surrounding airports [3]. Noise restrictions are often placed on airports (for example London Heathrow, Sydney Kingsford-Smith), which can limit daily operations [4].

Noise-efficient operations, such as Continuous Descent Approaches (CDAs), can significantly reduce the noise impact of landing aircraft by keeping aircraft at higher altitudes on approach to the airport and by reducing power during descent [5], [6]. Research into the economic and environmental costs and benefits of using continuous descent approaches (as opposed to step descent) showed significant reduction in noise footprints and aviation emission [7], [8]. CDA is also considered as one of the building blocks for Single European Sky ATM Research (SESAR) and Next Generation Air Transportation System (NextGen) [9], [10].

A typical CDA procedure starts from an Initial Approach Fix at approx. 10,000 ft to 8000 ft and around 30nm to 25nm to touchdown. When cleared for the CDA, the aircraft starts its descent in such a way that the ILS (Instrument Landing System) intercept point is reached at 2500ft - 2000 ft (Final Approach Fix) with idle or near idle power setting. This airspace is usually referred to as transition airspace. In CDA the aircraft descends to touchdown with a glide slope of 3 degrees along an optimized lateral flight path. In conventional CDA approach this lateral path is fixed.

Beside the need for a mandatory certification for pilots and aircrafts to conduct a CDA operation, the CDA routes are fixed and published well in advance. They are essentially routes that are vertically optimized. With the changing traffic conditions as well as noise abatement rules (to distribute noise evenly in surrounding areas or to shift it to uninhabited areas), the full benefits of CDA operations is not fully realized [11].

In this paper we propose a methodology to generate dynamic CDA routes. Dynamic CDA are aircraft specific, starting from Initial Approach Fix to Final Approach Fix. The word dynamic refers to the fact that two aircraft in the same approach airspace can follow two different trajectories: there is no standard arrival (STAR); in practice, each aircraft

will receive its dynamic CDA by datalink before starting its descent. These CDA trajectories are generated by discretizing the terminal airspace into concentric cylinders with artificial waypoints, and uses enumeration and elimination (based on aircraft performance envelope) from one waypoint to another to identify all the possible routes. For each transition a variety of metrics including noise, emission and fuel burn are computed. From the resulting set of possible CDA routes, those routes are identified that represent the best trade-off on the given objectives.

The proposed methodology is integrated into a high fidelity air traffic simulator (ATOMS) [12]. The methodology utilizes real time aircraft position and defined objectives to generate trajectories which can be converted into a set of artificial waypoints for continuous descent in transition airspace for a given set of objectives such as noise, emission and fuel consumption.

The dynamic CDA approach is developed with consideration for future integration with Flight Management Systems (FMS). To accommodate for real-time updates to the lateral path, the algorithm outputs a set of CDA trajectories with trajectory change points (TCPs) which represent the possible optimal trade-offs between competing objectives. These CDA trajectories can then be displayed to the approach/tower ATCs, where a controller can select a solution based on operational preferences and uplink the chosen trajectory to the aircraft.

The proposed methodology is then extended to multiple aircrafts scenario, by blocking the artificial waypoints generated for the first aircraft and making them inaccessible for other aircraft for a period of time based on estimated time of arrival (ETA) of the first aircraft at its respective artificial waypoints.

II. BACKGROUND

Environmental impacts due to aviation operations in the vicinity of airports have become a serious concern to the community [13]. Aircraft noise and emission have generated numerous complaints and public litigations from residents near airports. This is affecting the progress of commercial aviation, any efforts of airport expansion and new runway developments. The result is a lack of enough runways at major airports, which in turn increases fuel consumption and airspace congestion. This leads to increased aircraft emission, which affects both the natural environment and human health [14].

Researchers have been evaluating ways to alleviate noise and emission problems associated with increases in air traffic. Continuous descent approaches are noise- and fuel-efficient terminal approaches that have been a research topic over the last few years and are being explored by several governments, industry, and academic institutions.

A. Continuous Descent Approaches

A continuous descent approach is defined as "an aircraft operating technique in which an arriving aircraft descends from an optimal position with minimum thrusts and avoids level flight to the extent permitted by the safe operation of the aircraft and compliance with published procedures and

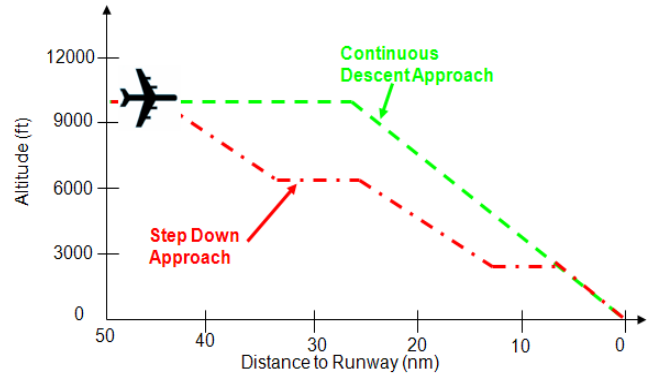


Fig. 1. A conceptual representation of step descent approach and continuous descent approach

ATC instructions." [15]. Thus in CDA, the descent is with no level altitude segments, which are common in traditional step-descent approaches. The goal of developing a CDA is to keep the aircraft thrust as low as possible and the aircraft at higher altitudes for as long as possible. An ideal CDA allows the engines to be at idle thrust during most of the descent. Figure 1 shows the conceptual representation of a conventional step descent approach and a continuous descent approach which starts typically at 10,000 ft and around 25-30 nm from touchdown point [7].

After the aircraft begins to descend past top of descent (TOD), lower thrust, fuel consumption and noise results from eliminating level altitude segments. In CDA operations, the thrust is near idle during most of the descent; therefore significant deceleration is achieved by using flaps.

CDA flight tests at Louisville International Airport in the US have shown a 50% reduction in acoustic energy, compared to traditional approach routes [8]. Significant fuel saving was also shown, which over time would greatly benefit both the environment and the airlines. CDA operations have been implemented at some airports, such as Heathrow in London, Schiphol in Amsterdam and Brisbane in Australia during low-density traffic operations.

III. DYNAMIC CONTINUOUS DESCENT APPROACH

In ideal conditions, the CDA route should be an optimized 3D trajectory which is generated and shared between controllers and the pilot in real time by taking into account noise, emission, traffic, and wind conditions. With increased onboard computing power, advances in digital data transmission and proposed real time data link between controllers and pilots (CDPLC), up-linking and down-linking of trajectories is possible [16]. This makes the realization of real time CDA route generation a near possibility.

In the near future, controllers will be able to define their objectives and their relative priority, and uplink them to the approaching aircrafts. An onboard system can then use them to generate one or many CDA trajectories which can then be down linked for ATC's approval.

Finding dynamic CDA trajectories in transition airspace can thus be seen as a path planning problem in three dimensions. In air traffic management this problem attains unique dimensions due to aircraft performance constraints posed on it in approach phase such as limited manoeuvrability (low thrust), speed restrictions and altitude constraints. Apart from the hard safety constraints, the other competing objectives are to minimize noise, emission, and fuel consumption.

A. Problem Search Space

As shown in Figure 2, we define the problem search space (transition airspace) as a set of five concentric cylinders (to equally divide transition airspace with 5 nm safety separation) with runway (touchdown point) at the center. The height of the transition airspace for research purpose is set to 10,000 ft and the radius to 25 nm. The outer most cylinder (denoted Ring 4) is of radius 25 nm (transition airspace radius (TAR)) with subsequent inner cylinders (Rings 3, 2, 1 and 0) spaced at equal distance as calculated in Equations 1. The outermost cylinder height is 10,000 ft corresponding to the start altitude of CDA and subsequent inner cylinders are vertically separated by 2000 ft. Thus the transition airspace is divided into 5 levels with each level divided into 2000 ft to give a typical jet aircraft enough vertical height to maneuver given low thrust setting.

$$RingRadius = \frac{TAR \times (Ring\ Number + 1)}{5} \quad (1)$$

Each cylinder has wedges that represent transition points from one level to another. These wedge points are spaced 1.5 nm apart from each other for safe separation between approaching aircraft [17]. The number of wedges for each cylinder and the angle between them are computed based on Equations 2 and 3.

The number of wedges for a given cylinder is calculated as follows:

$$Number\ of\ Wedges = \frac{2\pi \times Ring\ Radius}{Separation\ Distance} \quad (2)$$

The angle between the wedges is calculated as follows:

$$Wedge\ Angle = \frac{2\pi}{Number\ of\ Wedges} \quad (3)$$

Using a transition airspace radius of 25 nm and a separation distance of 1.5 nm, equations 1 and 2 give the number of wedge points as 104, 83, 62, 41, and 20 for rings 4, 3, 2, 1 and 0 respectively.

At 2000 ft before touchdown it is assumed that the aircraft follows the final approach path on the Instrument Landing System (ILS) glide scope and lands. The transition from one wedge point to other wedge point is based on individual aircraft performance parameters derived from Eurocontrol's Aircraft Database (BADA) [18]. All the wedge points on the outermost cylinder (representing the boundary of the transition airspace) are accessible for an approaching flight. Similarly all the wedge points on the innermost cylinder represent Final Approach Fixes that lead to ILS touchdown point.

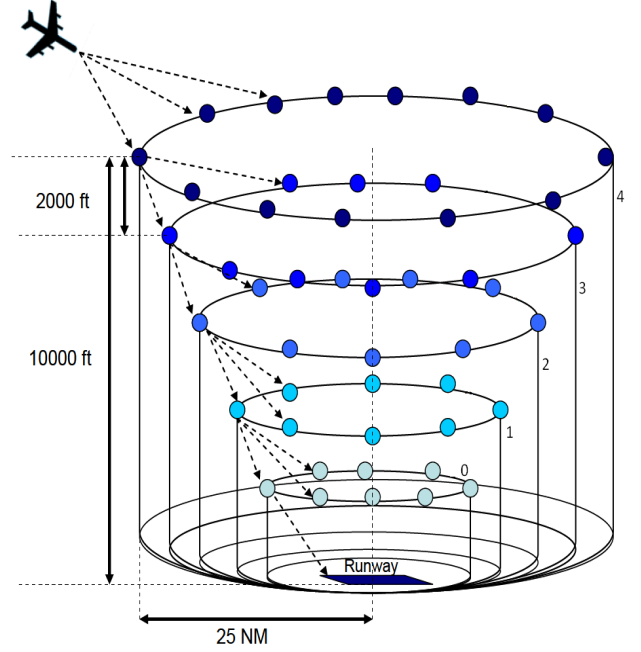


Fig. 2. Conceptual representation of division of transition airspace into concentric circles and wedges acting as trajectory change points for dynamic CDA trajectory generation.

From a given entry point (Initial Approach Fix) in the outer most ring and an exit point (Final Approach Fix) full enumeration of the search space can be performed. However, finding feasible solutions in such a large search space can be computationally expensive from safety and time perspective. If the number of states in the search space can be reduced without compromising solution quality, it will speed up convergence. When an aircraft approaches the Initial Approach Fix the search space is pre-processed based on the aircraft's performance envelope. This has two advantages: it reduces the search space, and it leads to a safety-inherent design for dynamic CDA route planning.

By pre-processing to eliminate infeasible transitions in the search space, the search is guaranteed to produce feasible solutions. We eliminate the state space recursively, starting from the entry point and doing forward enumeration on different layers. At each layer we eliminate states that violate the aircraft performance parameters, and then we move to the following layer. With each transition the objective values are computed and stored in the connecting node.

B. Problem Definition

The problem can then be stated as follows: Given a 3-D cylindrical grid (Transition Airspace) of dimensions i (ring), j (level), k (wedge), an entry point A (Initial Approach Fix) and a set of exit points B (Final Approach Fixes) find the set of routes (trajectories) between A and B that minimizes the given objectives (noise, emission and fuel).

This search space is then discretized in a cylindrical grid of $i \times j \times k$ wedge points, which forms the transition airspace

around the airport. Each cell in the grid forms a state in the search graph. The arcs of the graph represent possible transitions from one state to another. The state space is then processed by removing those states that violate aircraft performance parameters for continuous descent approaches, such as aircraft turn angle, maximum rate of descent, and speed constraints given the available thrust, using BADA.

The resulting three dimensional cylindrical grid is stored in a 3-D array data structure as an enumerated state space where each element of the array represents a point in the grid. The pseudo code for this is presented in Algorithm 1.

Algorithm 1 The pseudo code for state space processing

Require: Aircraft Performance Database D :(Rate of Heading Change, Rate of Climb and Descent, Altitude Ceiling, Max. Bank Angle, Max. Turn Angle, Max. Vertical Speed)
Grid G with $i \times j \times k$ dimensions
Exit node position in the grid(sink)

- 1: **for** Node in G **do**
- 2: Compute the turn angle, altitude change, rate of heading change required, rate of altitude change required, vertical speed required from each node (xyz) to the grid point (ijk) in G
- 3: **if** Transition from node xyz to grid point ijk violates D **then**
- 4: Eliminate the link
- 5: **else**
- 6: Retain the link
- 7: **end if**
- 8: **end for**
- 9: **return** Grid G with links within aircraft safety envelope

Every array element stores the information about its position (latitude, longitude and altitude) and all the immediate next links (that do not violate the aircraft performance envelope) from that point in the grid. Further, for each link the array element stores the heading change required, altitude change required, distance between the two, time, noise generated, emission generated, and fuel flow.

IV. OPTIMIZATION FUNCTION FORMULATION

We have considered three minimization objectives:

- Noise: The noise generated by the aircraft airframe for a given CDA trajectory;
- Emission: The emission generated by the aircraft for a given CDA trajectory;
- Fuel Burn: The fuel consumed by an aircraft for a given CDA trajectory.

Aircraft noise includes airframe noise and engine noise, but only airframe noise is calculated in this study because in most modern aircraft, airframe noise is a significant contributor to aircraft noise during the continuous descent approach. Sources of airframe noise include flaps, slats, wing, tails and landing gear [19]. Since during a CDA operation the engines are already on low thrust settings, and thus is a constant

contributor to the over all aircraft noise. The main source of variation is the airframe noise.

A. Noise Optimization Formulation

The objective function of the Noise optimization problem is a weighted integral of noise perceived at the ground level during the approach phase in the transition airspace. In particular, the weight factor considers the population and noise sensitivity of communities near an airport. Constraints on the optimization include initial and terminal conditions, the maximum feasible flap, velocity and altitude change rate, and a set of specified waypoints (wedge points) during the CDA. Therefore the noise optimization problem, to minimize noise given aircraft characteristics, could be formulated as follows:

$$\min f = \int_0^t W(t) \text{Noise}(V(t), h(t), \text{Flap}(t), t) dt \quad (4)$$

Where $W(t)$ is aircraft weight at time t , $V(t)$ is aircraft velocity at time t , $h(t)$ is aircraft altitude at time t and $\text{Flap}(t)$ is flap setting at time t .

The Overall Sound Pressure Level (OSPL) is a commonly used measure in acoustics studies [19]. The OSPL due to airframe noise is a function of altitude($h(t)$), velocity ($v(t)$), flap setting ($\text{Flap}(t)$), boundary layer thickness (b) and wingspan ($\delta(t)$) [20]. It can be expressed as:

$$\text{OSPL} = 50 \log v(t) - 20 \log h(t) + C_f \times \text{Flap}(t) + 10 \log \delta(t) \times b + \text{const} \quad (5)$$

During continuous descent approach, the altitude and velocity of the aircraft are decreasing gradually. Therefore, no abrupt noise changes occur. Thus we can define the noise cost function of the optimization problem in equation 4 as:

$$\text{Noise}_{ij} = W \times \sum_t [50 \log v(t) - 20 \log h(t) + C_f \times \text{Flap}(t) + 10 \log \delta(t) \times b + \text{const}] \quad (6)$$

where W is the weight factor.

B. Aircraft Fuel Burn Computation

Total approach fuel burn is estimated by integrating fuel burn at each second. Thrust specific fuel flow model of BADA with correction for aircraft mass was used. When the aircraft engine is set to idle thrust during approach and landing, the fuel burn per second is given by [18]:

$$\text{FuelRate} = \frac{C_{f3}}{60} \times \left(1 - \frac{3.2080 \times h}{C_{f4}}\right) \quad (7)$$

C_{f3} is 1st descent fuel flow coefficient and C_{f4} is 2nd descent fuel flow coefficient for an aircraft, derived from the BADA aircraft operation performance file.

The fuel flow for each transition is computed as:

$$\text{FuelFlow}_{ij} = \text{Time In Leg}_{ij} \times \text{FuelRate} \quad (8)$$

C. Aircraft Emission Computation

Four major aircraft emissions, CO_2 , HC , NO_x and CO are computed. The emission computation process is divided into two phases, below 3000 ft and above 3000 ft. Below 3000ft, the emission calculation is based on the ICAO Engine Exhaust Emissions Data Bank [21]. Above 3000 ft, the emission calculation is also based on the ICAO Engine Exhaust Emissions Data Bank, but emission factors are adapted to the atmospheric conditions at altitude by Boeing Emission Method 2 (BEM2) [22], which calculates emissions indices based on fuel flow and ICAO certification data. ICAO data at the four certified power settings at sea-level conditions is used to compute resulting emissions while correcting for atmospheric conditions. BEM2 computes flight emissions using, as a base, the measured fuel flow and the engine ICAO data sheets. It allows for ambient pressure, temperature, and humidity, as well as Mach number.

These emissions are formulated as

$$CO_2(g) = No\ of\ Engines \times EICO_2 \times FuelFlow(g/sec) \quad (9)$$

$$CO(g) = No\ of\ Engines \times EICO \times FuelFlow(g/sec) \quad (10)$$

$$HC(g) = No\ of\ Engines \times EIHC \times FuelFlow(g/sec) \quad (11)$$

$$NO_x(g) = No\ of\ Engines \times EINO_x \times FuelFlow(g/sec) \quad (12)$$

where $EINO_x$, $EICO$ and $EIHC$ are emission index of NO_x , CO and HC respectively, derived from the International Civil Aviation Organization (ICAO) Engine Exhaust Emission Data Bank, and $EICO_2 = EICO_{2,ideal} - \frac{44}{28}EICO$ where $EICO_{2,ideal}$ is 3156g and 44/28 ratio represents their different molar masses.

Respective emissions for each transition in the cylindrical grid (from node i to node j) are computed as:

$$Emission_{i,j} = Time\ In\ Leg_{i,j} \times Emission \quad (13)$$

We have used Nitrogen monoxide NO_x emission as the objective value for emissions. However, other pollutants (HC , CO and CO_2) computed in the study could also be used. We chose NO_x because of its impact on local air quality as well its major influencing substances on global warming [23]. NO_x is a precursor of ground-level ozone (O_3), hence an elevated O_3 level may result through a chemical reaction with oxygen at the presence of sunlight [23]. Respiratory complaints are the main effects related to elevated concentrations of NO_x around the airport area [24].

The overall optimization function F can then be stated as:

$$\min F = \sum_i \sum_j Noise_{i,j}, Emission_{i,j}, Fuel_{i,j} \quad (14)$$

V. AIRCRAFT PERFORMANCE MODEL

The following changes were made in the aircraft performance model of ATOMS to implement CDA approaches and to improve the fidelity of the simulation.

A. Final approach speed

The minimum landing speed, V_{min} , is now calculated as follows:

$$V_{min} = 1.3 \times V_{stall} \sqrt{\frac{m}{m_{ref}}} + 10.0kts \quad (15)$$

where 1.3 is a factor recommended by the BADA manual for all aircraft operations, V_{stall} is the stall speed at the reference mass m_{ref} , and m is the simulated aircraft mass.

B. Deceleration rate

The BADA manual recommends a maximum longitudinal acceleration/deceleration of $2.0ft/s^2$ (118 kt/sec), and this value was previously implemented in ATOMS as the maximum deceleration regardless of flight-path angle. To compensate for a descending aircraft, $g\gamma$ was subtracted from the maximum longitudinal acceleration, where g is the acceleration due to gravity in kts per second (kt/sec) and γ is the flight path angle in radians; for a 3 degrees flight path angle, the $g\gamma$ term is approximately equal to 1.0 kt/sec. This change was necessary to properly simulate the diminished deceleration capabilities that are characteristic of CDA operations.

The deceleration rates are also affected by the flap configuration. BADA aircraft-specific flap configuration for approach and landing and corresponding stall speeds were used. The landing-gear was fixed at 3000 feet and was reflected in increased coefficient of drag during landing.

C. Descent Thrust

Once the aircraft has descended below 10,000 ft it changes configuration as soon as the airspeed falls below threshold V_{min} . At the same time the thrust setting is also changed as follows:

if $h < 10,000$ ft and $V < V_{min} + 10.0$ kts

$$T_{des,ld} = C_{Tdes,ld} \times \left(\frac{m}{m_{ref}} \times T_{maxclimb,ISA} \right) \quad (16)$$

where $C_{Tdes,ld}$ is the landing thrust coefficient (dimensionless), m_{ref} is the reference mass of aircraft (tonnes) h (ft) is the aircraft altitude, $T_{maxclimb,ISA}$ is the maximum climb thrust at standard atmosphere conditions, which is computed as follows:

$$T_{maxclimb,ISA} = C_{Tc,1} \times \left(1 + \frac{h}{C_{Tc,2}} + C_{Tc,3} \times h^2 \right) \quad (17)$$

where $C_{Tc,1}$, $C_{Tc,2}$, and $C_{Tc,3}$ are aircraft specific maximum climb thrust coefficients in Newton, feet, $1/feet^2$ respectively.

VI. EXPERIMENTS & RESULTS

The transition airspace and CDA procedure was modeled in ATOMS, and experiments were conducted to evaluate the methodology.

For the single flight, a B737-400 aircraft on a flight from Melbourne to Sydney, arriving at Sydney Terminal Area with 34L as arrival runway, was simulated in descent phase. The aircraft is equipped with two CFM56-3C-1 engines with a

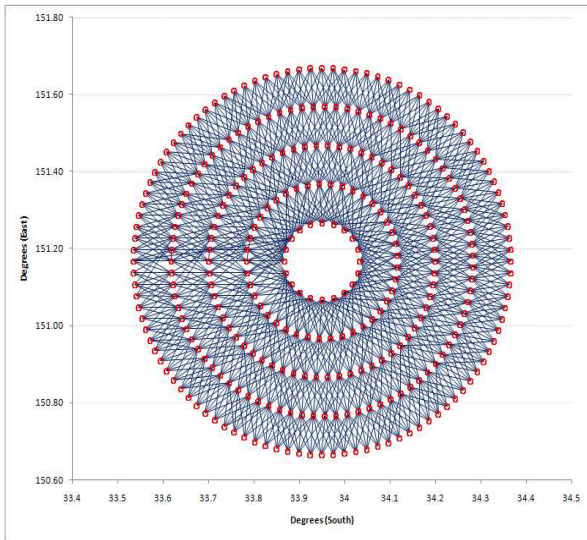


Fig. 3. The wedge links in the cylindrical transition airspace before removing the infeasible states.

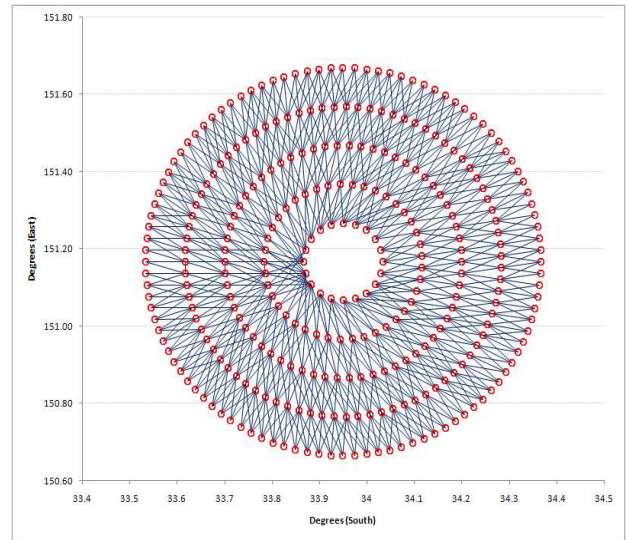


Fig. 4. The wedge links in the cylindrical transition airspace after removing infeasible states.

nominal weight (58000 kg). Two flap settings (15 degrees and 30 degrees) were used. ISA (International Standard Atmosphere) conditions are assumed for performance, fuel, noise and emission calculations. ISA defines air temperature, pressure and temperature as well as other atmospheric parameters as functions of altitude. Neither local deviations from ISA conditions nor winds are considered for our experiment purpose.

A single aircraft was investigated first. The algorithm was used to identify a set of possible dynamic CDA trajectories. The dynamic CDA routes were then compared on noise, emission and fuel burn with same flight conducting a typical fixed CDA procedure (MANFA ONE Arrival) at Sydney airport. The results of this experiment are presented in this section of the paper.

A second experiment investigated a scenario with multiple flights performing CDA operation, to gain insight into the throughput capacity of transition airspace. Those results are presented in Section VII.

A. Dynamic CDA Trajectories

Once the aircraft is in descent mode after top of descent, 25 nm before the transition airspace, the algorithm searches for possible wedge points on the transition airspace boundary. The algorithm computes the entry wedge point (Initial Approach Fix) that has least distance between the aircraft and the wedge points of outer most cylinder and that involves minimum aircraft heading change.

It then determines the exit wedge points (Final Approach fixes) that can be achieved from the IAF. For research purpose the runway is assumed to be the center point of the concentric rings, thus all the points on the innermost circle become the target set for exit. We first demonstrate the generation of transition airspace and the fully enumerated state space. Figure 3 shows all the possible wedge links in the cylindrical

transition airspace before removing infeasible states (top) and after removing infeasible states (bottom). Figure 4 illustrates the significant reduction in the state space after processing it by removing those links that violate aircraft performance constraints.

Based on the IAF point, all the possible paths are generated. For each TCP in a path, the emission, noise and fuel values are computed as described above, and these are aggregated for each CDA trajectory. There were 11,254 possible routes generated from the 104 wedge points on the outer most ring to the 20 wedge points on the inner most ring. From every wedge from the outermost ring there is a unique path that leads to final approach fix points in inner most ring, because the choice of entry wedge point (IAF) for the aircraft is based on which point is closest to it that requires the least deviation from current flight track.

The aircraft has ring 4, level 4, wedge 14 as the closest IAF. The methodology generates 101 possible solutions (dynamic CDA trajectories) for the aircraft from the selected IAF (starting from 4-4-14) to all the possible exit points (FAF) in the given transition airspace. Figure 5 shows the 3D view of all the CDA trajectories starting from the transition airspace entry point (IAF) to the final approach point (FAF), which is 2000 ft above touchdown.

Out of 101 possible dynamic CDA trajectories, 4 trajectories were “non-dominated solutions”. The concept of “non-dominated” [25] is generally used to compare two solutions a and b : If $f(a)$ is no worse for all objectives than $f(b)$ and wholly better for at least one objective it is said that a dominates b . A set F of solutions is said to be a non-dominating set if no element of the set dominates any other. These solutions are also called Pareto-optimal, as no other feasible solution dominates them. The set of all Pareto-optimal solutions is known as the Pareto set, P ; solutions in the Pareto set represent the possible trade-offs between competing

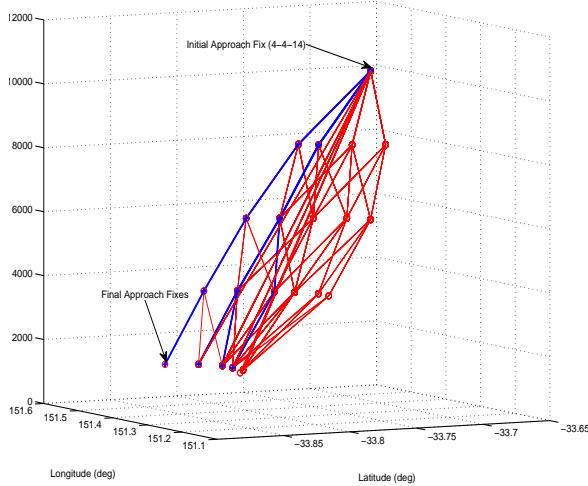


Fig. 5. 3D view of dynamic CDA trajectories generated from one of the entry point (4-4-14) in the transition airspace by the algorithm. The figure also highlights the four non-dominated trajectories.

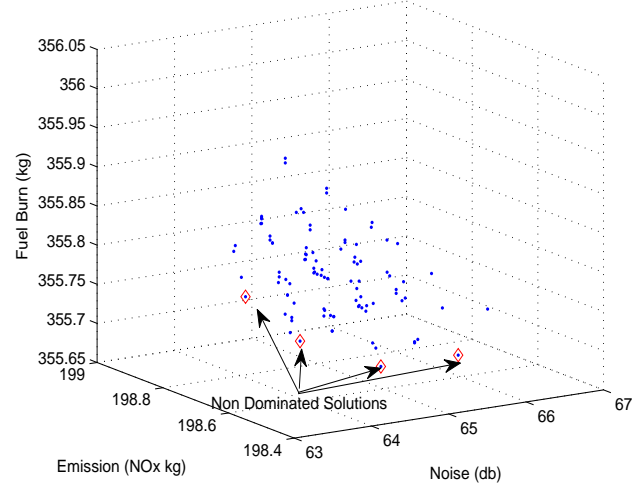


Fig. 6. 3-D plot of the three objective values (fuel, emission and noise) for all the feasible dynamic CDA trajectories. The four Pareto-Optimal solutions are highlighted by red diamonds.

TABLE I

OBJECTIVE VALUES OF FOUR PARETO-OPTIMAL SOLUTION TRAJECTORIES OUT OF 101 CDA TRAJECTORIES GENERATED BY THE ALGORITHM.

Route (Ring-Level-Wedge)	Noise (db)	Emission NO_x (kg)	Fuel (kg)
4-4-14 3-3-11 2-2-8 1-1-4 0-0-0	63.56	198.68	355.77
4-4-14 3-3-11 2-2-8 1-1-5 0-0-1	64.01	198.62	355.72
4-4-14 3-3-11 2-2-8 1-1-5 0-0-2	64.97	198.60	355.67
4-4-14 3-3-12 2-2-9 1-1-6 0-0-3	65.97	198.60	355.67

objectives.

Mathematically it can be stated as [26]: a vector $\mathbf{u} = (u_1, \dots, u_m)$ is said to dominate \mathbf{v} if and only if $\forall i \in \{1, \dots, m\}, u_i \leq v_i \wedge \exists j \in \{1, \dots, m\} : u_j < v_j$. Thus a solution $x \in N$ is said to be non-dominated or Pareto-optimal with respect to the whole set N if and only if there is no other solution $x' \in N$ for which $F(x')$ dominates $F(x)$. Figure 5 illustrates the non-dominated solution trajectories among the set of all feasible trajectories.

The Pareto solution set and their route indexes are presented in Table I. “Ring” in Table I implies the cylinder number where 4 is the outer most and 0 is the inner most cylinder. “Level” implies the altitude level, with 4 representing 10,000 ft and 0 representing 2000 ft. The aircraft chooses any one of the non-dominated solutions and after reaching the final approach point the aircraft descends directly to the designated runway.

Table I also shows the objective values for each of the four trajectories. It shows the emission, fuel flow and noise for each representative CDA trajectory. Each CDA route generated by the algorithm has some trade off between noise, emission and fuel consumption. Figure 6 shows the 3-D plot for the three objective values for all the feasible solutions as well as the Pareto-optimal solutions.

The CDA trajectories generated are within the aircraft performance bounds. Figure 7 shows the altitude, flap configurations, thrust, speed profile, fuel flow and acceleration from 80nm till touchdown for one of the Pareto-Optimal dynamic CDA trajectories. 15 degree flaps were extended at approximately 10 nm to threshold and 30 degree flap were extended at approximately 7 nm to threshold, and thrust is almost idle until 23 nm to touch down. The aircraft under goes deceleration many times, as compared to step down approach, to maintain the required speed profile. The generated trajectory maintains the 3-degree flight path angle with speed and altitude constraints while executing the selected CDA approach.

B. Comparison of Dynamic CDA Trajectories with Fixed CDA Trajectory

We compared the performance (measured on noise, emission (NO_x) and fuel) of Dynamic CDA trajectories with the fixed CDA trajectory flown using a STAR route for the Sydney (Kingsford-Smith Airport) “MANFA ONE” arrival.

As shown in Figure 8, we modeled the “BOREE-BEROWOVILS-MAJAR-MANFA-JAKLN-LISHA-SUZAN” STAR route in the ATOMS simulator. The aircraft follows the STAR route using continuous descent approach and lands east of runway 16R/34L. Same experiment and flight settings were used as for dynamic CDA trajectories.

To generate the dynamic CDA trajectories, Ring 4 Level 4 Wedge 68 (4-4-68) is chosen as the transition airspace entry point (IAF) for the inbound aircraft, as it coincides with the fixed CDA entry point for MANFA ONE Arrival STAR fix at an altitude of 10,000 ft. From this IAF point until the final approach fix (2000 ft) the noise, emission and fuel burn are computed and compared for the two approaches. Figure 9 shows the fixed CDA trajectory for Sydney MANFA ONE arrival as compared to the non-dominated solution trajectories

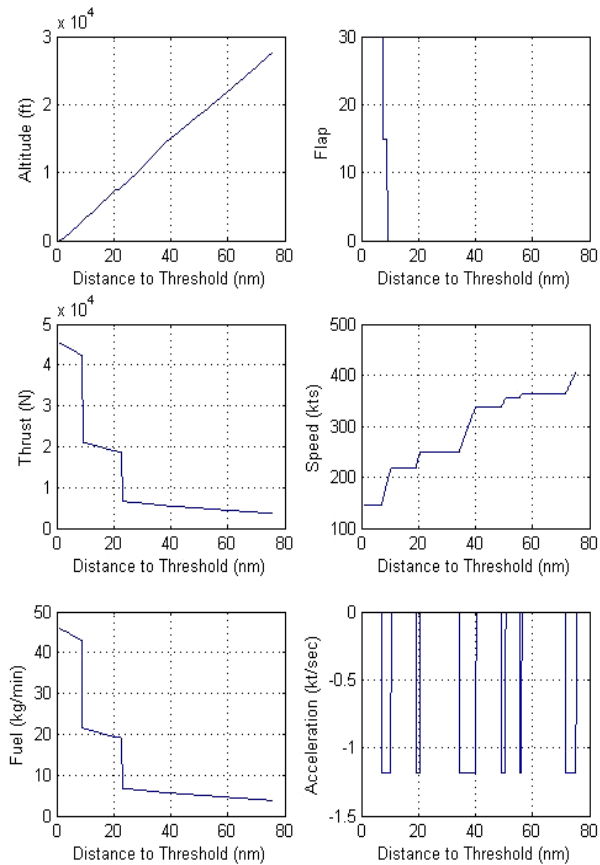


Fig. 7. Distance to threshold plots for aerodynamic parameters and fuel flow for continuous descent approach trajectory (80 nm to touchdown) for one of the CDA trajectories.

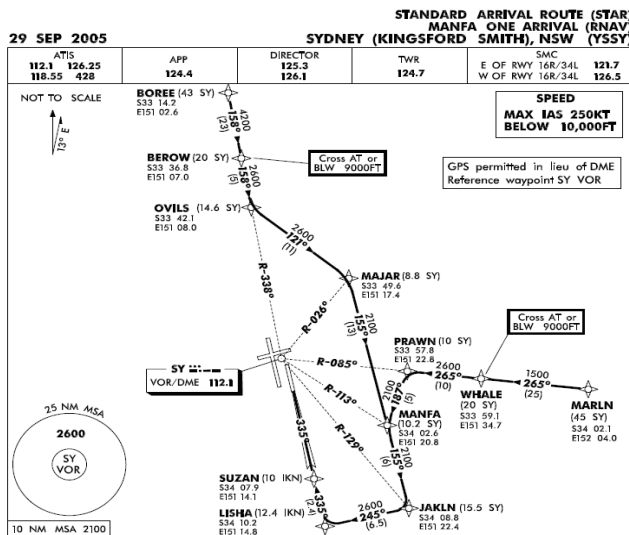


Fig. 8. STAR chart of MANFA ONE arrival [27] at Sydney International Airport, which is modeled in ATOMS for CDA procedure simulation.

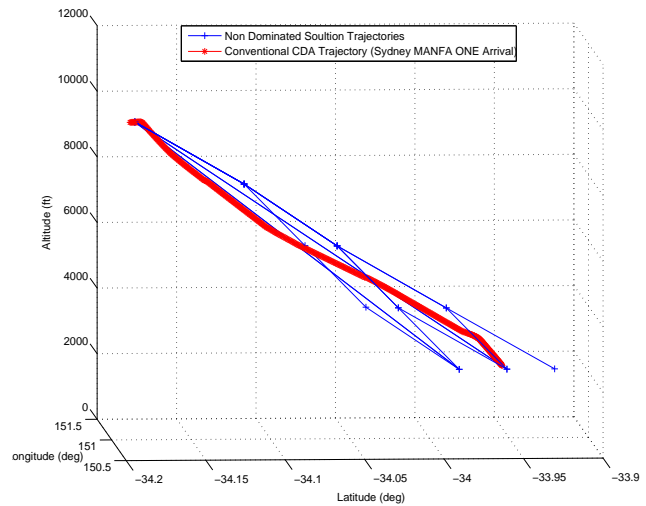


Fig. 9. Conventional CDA trajectory for Sydney MANFA ONE arrival as compared to the Non-Dominated solution trajectories generated by the algorithm.

TABLE II
OBJECTIVE VALUES OF FIVE NON-DOMINATED SOLUTION TRAJECTORIES OUT OF 67 CDA DYNAMIC TRAJECTORIES GENERATED BY THE ALGORITHM FOR ENTRY POINT 4-4-68 CORRESPONDING TO MANFA STAR FIX.

Route (Ring-Level-Wedge)	Noise (db)	Emission NO_x (kg)	Fuel (kg)
4-4-68 3-3-55 2-2-41 1-1-27 0-0-14	64.99	198.60	355.69
4-4-68 3-3-55 2-2-42 1-1-28 0-0-14	63.98	198.61	355.69
4-4-68 3-3-55 2-2-42 1-1-28 0-0-15	63.52	198.64	355.73
4-4-68 3-3-55 2-2-42 1-1-29 0-0-15	63.02	198.66	355.73
4-4-68 3-3-55 2-2-42 1-1-29 0-0-16	62.57	198.69	355.78

TABLE III
COMPARISONS OF NOISE, EMISSION AND FUEL VALUES OF ONE OF THE NON-DOMINATED TRAJECTORIES OF DYNAMIC CDA WITH TRADITIONAL CDA USING FIXED STAR ROUTE.

Route	Noise (db)	Emission NO_x (kg)	Fuel (kg)
Dynamic CDA	64.99	198.60	355.69
Fixed Route CDA	76.43	225.68	361.21
Reduction (%)	14.96	11.99	1.5

generated by the algorithm.

Dynamic CDA approach generated 67 possible routes from IAF point (4-4-68) to final Approach fixes. Out of them five were non-dominated solution trajectories on noise, emission (NO_x) and fuel burn objectives. Table II shows the five non-dominated solution trajectories and their objective values.

Table III compares one of the non-dominated dynamic CDA routes with the fixed CDA route on the noise, emission and fuel burn objectives and illustrates the savings achieved by the former approach.

For the Dynamic CDA we see a reduction of 14.96% in airframe noise, 11.99% reduction in NO_x emission and 1.5% reduction in fuel burn. Though the savings in fuel burn was

not that large, since the aircraft was already in low thrust setting and there was not much room for reduction, from environmental prospective the reduction was still important.

VII. MULTIPLE AIRCRAFT SCENARIO

CDA operations are usually conducted at night and/or in low traffic conditions. One reason is that for CDA, the landing interval has to increase to guarantee sufficient spacing between aircraft on the final landing segment [28]. The increased landing interval is necessary because of the large dispersion in aircraft approach speeds. Moreover, since the aircraft conducting CDA operation is in ideal or near ideal thrust, the increased spacing allows for thrust increase to deal with sudden changes in wind, missed approaches or any other reason that requires vectoring the aircraft.

For the proposed dynamic CDA methodology, we looked into different air traffic scenarios with 100 flights each having different activation timings and traffic distributions. We then evaluated the performance of the proposed methodology in terms of throughput capacity, delay between outer marker and initial approach fix, delay between initial approach fix and final approach fix as well as cumulative values for emission, noise and fuel.

A. Sequencing Multiple Flights

We incorporated a delay algorithm, which uses the estimated time of arrival (ETA) of the flight at its designated IAF and then at each artificial waypoint in the transition airspace until the FAF, to sequence the flights. A time window is assigned based on aircraft type (light, medium, heavy) at each artificial waypoint, so that any subsequent flights does not occupy the same waypoints in that given time frame. This is achieved by time-blocking these waypoints, which are then eliminated during the link enumeration process. This ensures that no two flights occupy the same waypoint in a given time window.

The dimensions of the cylindrical grid (transition airspace) are fixed, but the links (and their objective values) from one level to the other and from one wedge to the other are always specific to an aircraft. Aircraft are allocated the CDA route on First Come First Serve (FCFS) basis. If the route is not available, the aircraft is slowed down by 20 knots if the speed is within its flight envelope (stall speed). Otherwise the aircraft is put on hold. Figure 10 illustrates the time delay algorithm component in the dynamic CDA generation process.

There are four main components of the time delay algorithm:

- Selecting a flight: A flight is selected for CDA route allocation when it reaches the outer marker (50 nm from IAF) using First come First Serve (FCFS). This is based on the flight’s ETA at the destination airport.
- Selecting an IAF: An IAF is selected based on minimum distance, and minimum flight path deviation. The selected IAF is checked for availability (whether open or closed) in the time window, given the aircraft’s ETA at that IAF. If the IAF is not available another possible IAF is selected.

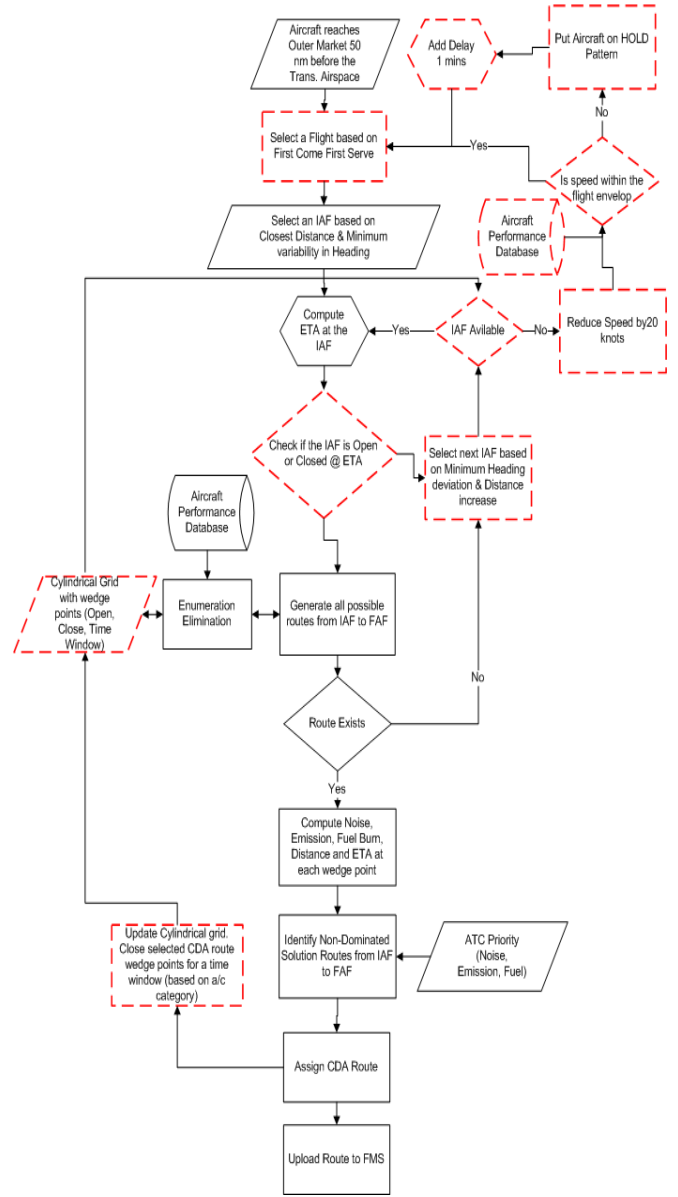


Fig. 10. Flow chart showing the Delay algorithm components (red dotted) in the Dynamic CDA generation process

- Adding Delay: If no IAF is open, given the Flight’s ETA at any of the IAF, the algorithm generates a “REDUCE SPEED” command. It then checks whether the reduced speed is within aircraft stall limits given the altitude and flight phase (approach/descent). If the proposed speed is with stall limits then ETA at the destination is recalculated and the flight is re-positioned in the FCFS list. Otherwise the aircraft is set in HOLD status i.e. “Frozen” in simulation. However, the flight parameters including noise, emission, fuel are continuously computed during the hold process.
- Updating the Cylindrical Grid wedge points: Based on the selected CDA route for the flight, the algorithm updates the cylindrical grid for all the wedge points (artificial

TABLE IV
TIME BASED SEPARATION FOR CDA ARRIVALS [29] AT EACH OCCUPIED WEDGE POINT BETWEEN LEADING AND FOLLOWING AIRCRAFT IN THE CYLINDRICAL GRID.

↓ Lead AC / Follow AC →	Heavy	Medium	Light
Heavy	90 sec	110 sec	145 sec
Medium	70 sec	70 sec	125 sec
Light	70 sec	70 sec	70 sec

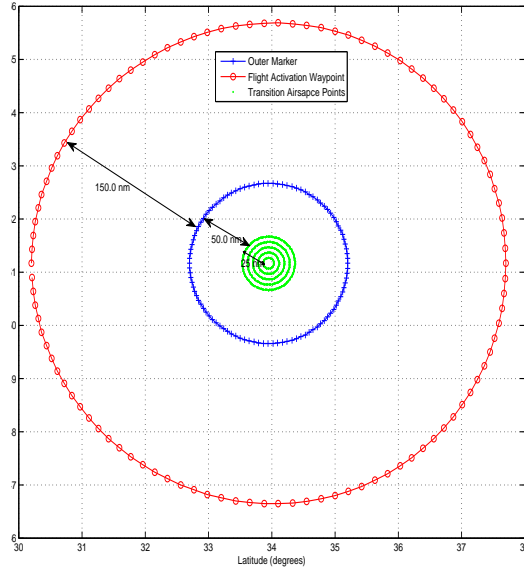


Fig. 11. Optimization Airspace showing activation points, which are 150 nm from the outer marker, outer marker points which are 50 nm from the Initial Approach Fix.

waypoints) that form part of the dynamic CDA route. We have used time based separation [29], where the algorithm sets the wedge point as closed and assigns a busy status (for the ETA of the flight and the wake separation criterion) as shown in table IV. Once the aircraft crosses the waypoint the status is set to open.

For the experiments we have only used heavy aircraft, where the separation between the two is taken as 90 seconds.

B. Traffic Distributions

Figure 11 illustrates the overall airspace where the activation point is set to 150 nm from the outer marker. The outer marker is 50 nm away from the initial approach fix. The flights get activated at their designated activation point based on the traffic distribution. Once the flight reaches the outer marker the optimization process starts.

As illustrated in figure12, three traffic distributions have been developed to get variation in arrival traffic distribution. The traffic distributions are generated using a probability distribution function. The circular grid is divided into 8 equal regions, 45 degrees each, which we call Octants.

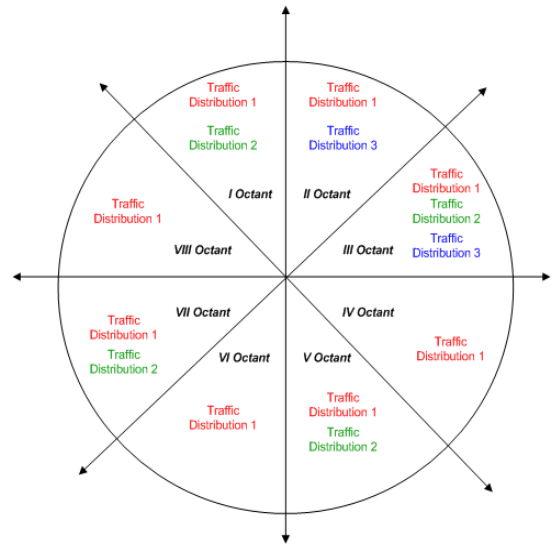


Fig. 12. The traffic distributions of incoming traffic in eight Octants.

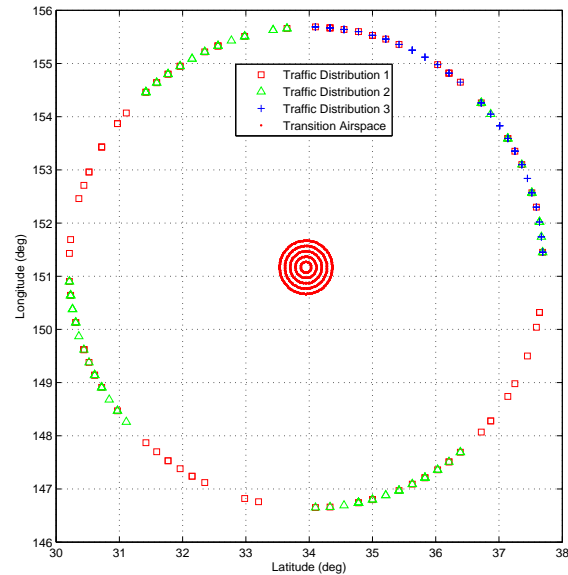


Fig. 13. The flight activation positions for the three traffic distributions in the eight octants .

- Traffic distribution 1: All the incoming traffic is uniformly distributed in all the eight Octants.
- Traffic distribution 2: The incoming traffic is uniformly distributed in Octants II, IV, VI and VIII
- Traffic distribution 3: All the incoming traffic is uniformly distributed in Octants II and III.

Figure 13 illustrates the flight activation points for the three traffic distributions in experimental airspace.

C. Activation Time

Flight activation time is based on inter arrival time. We have used four intervals, based on the heavy-heavy aircraft

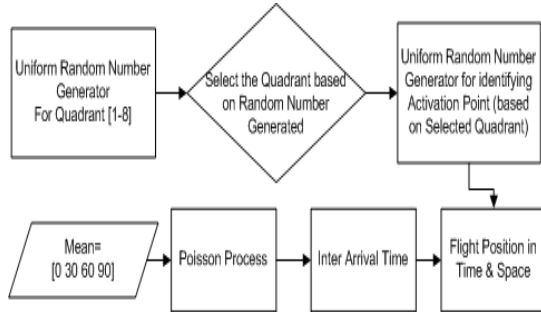


Fig. 14. Process showing the generation of Flight position in space and time based on Traffic Scenario.

separation of 90 seconds. The activation time is generated using a Poisson process with value of m set to 0, 30, 60, 90. If inter arrival time is 0, this implies that all the flights are activated at the same time.; an inter-arrival time of 30 implies the next flight activation time is poisson distributed with mean 30 seconds; and so on.

The combination of three traffic distributions and 4 activation time distributions gives us 12 air traffic scenarios, each of 100 flights.

As illustrated in Figure 14, a uniform random number generator first selects the Octant (from 1 to 8) based on the Traffic Scenario, for example, if the traffic distribution is 3 then it only select points from Octant II and III, else will regenerate the random number. There are 104 activation points equally divided in the eight Octants, so there are 13 points in each Octants. Once the octant is identified, it will then select the activation point using a uniform random number. Thus, if octant I is selected by above process then a uniform random number generator will select an activation point [0-12] for a flight in this octant.

As an example, Figure 15 shows the ATOMS simulation snapshot for one of the scenarios (Evenly distributed traffic in space, and inter arrival time=0).

D. Results and Analysis

We collected three metrics for dynamic CDA operations in a high density traffic environment, for each of the 16 scenarios described above (recall that each scenario involves the same number and same type of aircraft):

- Throughput of Transition Airspace (Flights per minute): This gives the number of flights that can be processed by the system per minute. It is estimated by dividing the number of flights processed by the system by the time difference between first flight activation time and last flight landing time.

$$\text{Throughput} = \frac{\text{Flights}}{\text{ActivationTime}_{FF} - \text{LandingTime}_{LF}} \quad (18)$$

where FF implies the first flight activated in the scenario and LF implies last flight which landed in the scenario.

- Flight Delay (From Outer Marker to Initial Approach Fix (IAF): This is the average flight delay time from

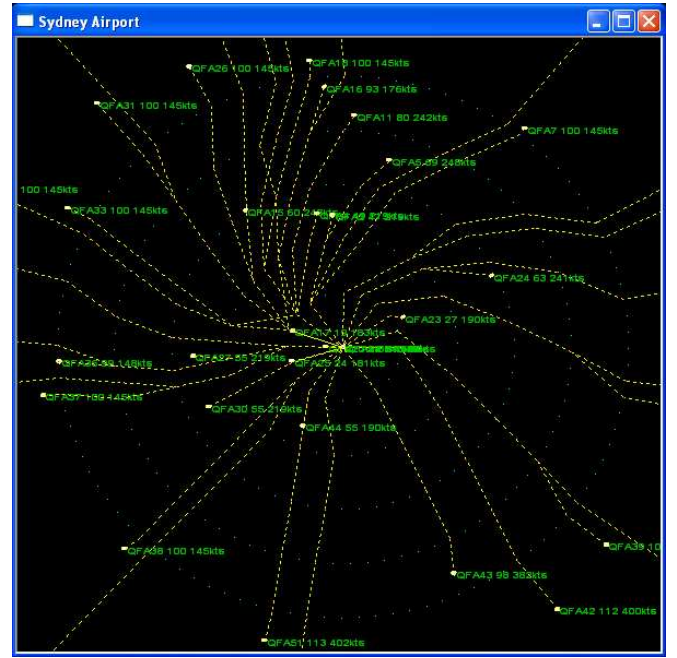


Fig. 15. Snapshot of traffic scenario simulation in ATOMS for evenly distributed traffic in space and inter arrival time = 0

Outer Marker to IAF, and is a measure of HOLD induced delay. It is estimated by taking the difference between the ETA (Estimated time of arrival) of flight to the IAF and ATA (Actual Time of Arrival) to the IAF from the outer marker, averaged over 100 flights.

$$\text{Delay} = \left[\frac{1}{N} \sum_{i=1}^{100} (ATA_i - ETA_i) \right]_{IAF}^{OM} \quad (19)$$

- Noise, Emission and Fuel burn: The cumulative Noise, Emission (NOx) and Fuel burn for all 100 aircraft. This is collected from the the Outer Market till final approach fix.

1) *Throughput*: Figure 16 shows the throughput of the system for the three traffic distributions with different inter arrival timings. It can be seen that when the inter arrival time is 0, then Traffic distribution 2 (Traffic distributed in alternate octant) gives the best throughput. As expected traffic scenario 3 where all the flights are from octant 3 and 4 has the least throughput.

However, interestingly, when the inter arrival time between flights is increased to 30 sec scenario 3 gives the best throughput. With 90 sec of inter arrival timing the traffic distribution do not make much difference in the throughput of the system.

2) *System Delay*: Figure 17 shows the average flight delay from Outer Marker to Initial Approach Fix for different inter arrival timings for the three traffic distributions.

It can be seen that for traffic distribution 3, (a typical morning scenario when all the oceanic flights from Americas are lined up for entry into Sydney TMA), the average flight delay is highest with the inter arrival timings of 0 and 30 sec. By increasing the inter arrival time to 60 sec scenario 3

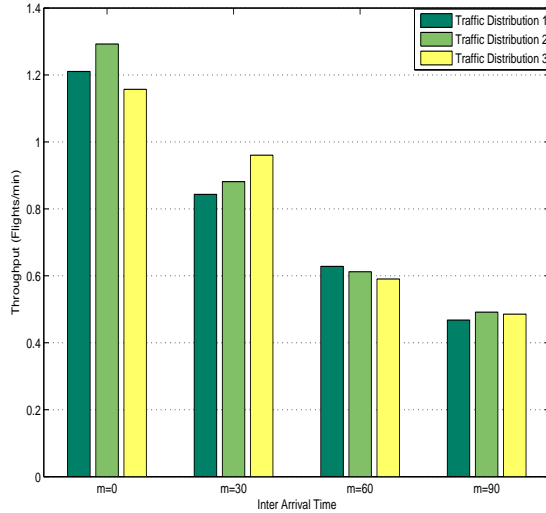


Fig. 16. Throughput of the transition airspace for the three traffic distributions with different inter arrival timings.

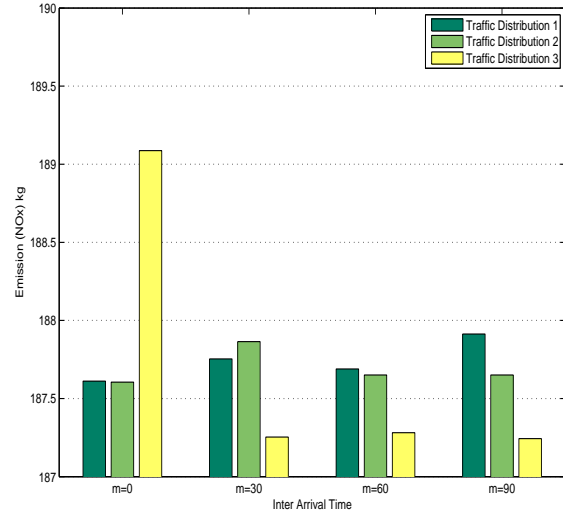


Fig. 18. Cumulative emission (NOx) from the outer marker to the final approach fix.

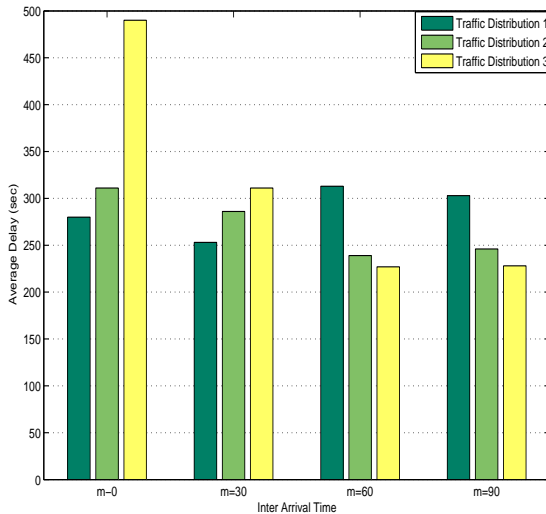


Fig. 17. Delays (sec) from the Outer Marker to IAF for the three traffic distributions with different inter arrival timings.

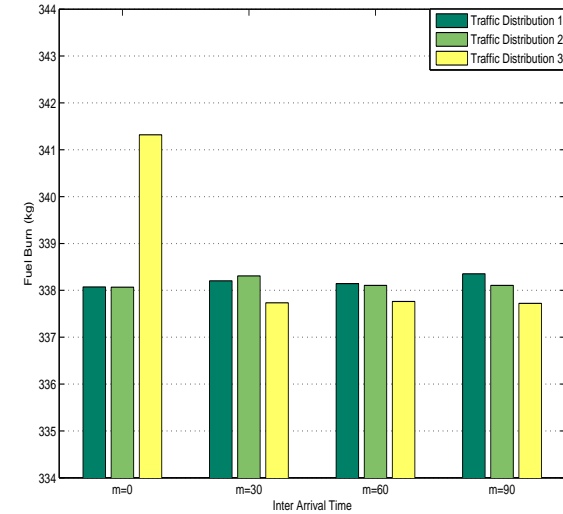


Fig. 19. Cumulative fuel burn from the outer marker to the final approach fix.

gives the least delay and the delay in scenario 1 is significantly increased. For an evenly distributed traffic (Traffic Distribution 1) the best performance is achieved with 30 sec of inter arrival time.

3) *Cumulative Noise, Emission and Fuel burn:* Figure 18, Figure 19 and Figure 20 shows the cumulative Emission (NOx), Fuel burn and Noise for the three traffic distributions with different inter arrival timings respectively. For NOx emissions, Traffic distribution 3 shows highest emission for inter-arrival time of 0, as it results in highest hold patterns, leading to higher fuel burn and emission. However with increased inter arrival timings of 30, 60 and 90, this scenario gives the least

emission. A similar pattern is reflected in fuel burn for the three traffic distribution, with traffic distribution 1 and 2 giving similar performance. In terms of noise, Scenario 3 remains highest noise contributor, this can be explained by the fact that this scenario requires more spiral routing pattern in the transition airspace to accommodate for the highly concentrated traffic in one area.

VIII. CONCLUSION & FUTURE WORK

The proposed methodology to generate aircraft-specific dynamic CDA routes that are both laterally and vertically optimized on given objectives (noise, emission and fuel) from

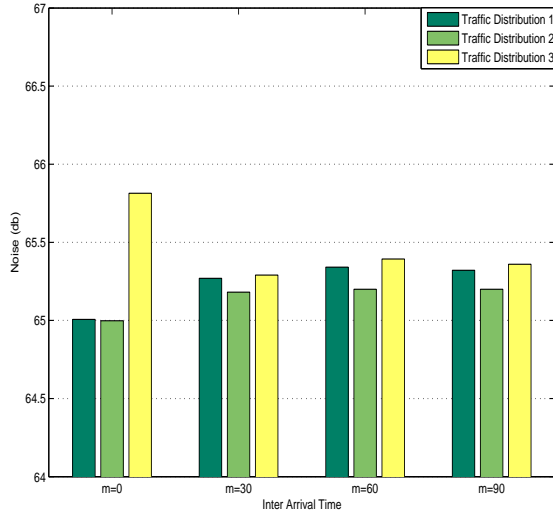


Fig. 20. Cumulative noise from the outer marker to the final approach fix.

an Initial Approach Fix IAF (10,000 ft) to Final Approach Fix FAF (2000 ft) demonstrates that significant savings can be achieved as compared to fixed CDA routes. The use of real-time aircraft position and performance parameters leads to inherently safe CDA routes which can then be converted into a set of artificial waypoints for continuous descent in transition airspace.

The methodology uses the concept of non-dominated solutions, where all the routes in this set show the trade-off between the competing objectives of noise, emission and fuel burn. By assigning desired weights based on operational priority of each objective and using a simple search algorithm, the desired route can be selected for uplink to the aircraft's FMS. These waypoints can then be fed to the FMS of the flight and autopilot can execute the CDA manoeuvre.

Another benefit of dynamic CDA with cylindrical representation of transition airspace in rings, levels, and wedges is that it can be easily used for the distribution of aircraft noise in areas surrounding the airport. This can be achieved by blocking a set of wedge points that are to be avoided while generating the set of alternative routes from initial approach fix to final approach fix. This can also be extended to incorporate thunderstorm cells in the vicinity of the airport, however dynamic blocking of wedge points based on heading, speed and radar reflectivity of thunder storm cells will be challenging.

The proposed methodology is also extended to accommodate for multiple-aircraft scenario by using time delay algorithm. 12 different traffic scenarios from three different spatial distribution of traffic and four different inter arrival time distribution derived from a poisson process were investigated on throughput, delay, emission, noise and fuel. The results gives interesting insight into the interplay of spatial and temporal distribution of traffic and inter-arrival time and its

consequence on throughput and delay of the system.

The dynamic CDA approach has its challenges. It depends largely upon aircraft performance i.e. meeting speed and altitude restriction, within the given time of arrival, at artificial waypoints while making a continuous descent. On the operational side it may lead to reduced Controller-Pilot communications for level-off segments, but may increase communications for speed constraints. Further co-ordination between approach and tower controller to achieve dynamic CDA, especially in a traffic constrained environment, will be a challenging task. On the ATC side there can be a lack of flexibility, since the clearance for the approach has to be given well prior to the IAF. In the circumstance that a CDA needs to be aborted, it is impossible to resume it and further radar vectoring will have to be used.

For future work we will be using demographic data to study the alternative strategies for noise distribution in the community. The impact of emission on local air quality and means to alleviate it will be investigated by incorporating the Emission Dispersion Model. Wind information will be used by storing the wind data in the wedges, and the effect of head-wind and cross-winds will be incorporated in dynamic CDA trajectory generation. We will also be looking into Approach and Tower controller coordination issues in implementing dynamic CDAs.

Another challenge lies in implementing CDA operation in a mixed equipage aircraft environment, where aircraft with or without different capabilities (CDPLC, ABS-B, CDTI etc.) all want to land at the same airport. How to accommodate such heterogenous traffic with mix of approach procedures (CDA, Step Descent, etc.) will be an interesting research question.

Dynamic CDA trajectory is a step towards realization of 4D trajectory management in approach and descent phases of flight. Given the inherent uncertainties in air traffic environment and changing objectives of the ATCs, pre-published routes with fixed CDA altitude profiles may not be able to realize the full potential of CDA. Dynamically generated flexible CDA trajectories that are aircraft-specific and are optimized on given objectives (noise, fuel, emissions), that satisfy hard constraints of aircraft performance during descent and approach, and that can meet air traffic constraints (traffic, weather) can provide more efficient use of airspace and increase airport throughput capacity.

ACKNOWLEDGMENT

This work has been co-financed by the European Organisation for the Safety of Air Navigation (EUROCONTROL) under its University Research Grant programme. The content of the work does not necessarily reflect the official position of EUROCONTROL on the matter.

REFERENCES

- [1] G. Donohue and W. Laska, "United States and European Airport Capacity Assessment using the GMU Macroscopic Capacity Model (MCM)," in *Proc. 3rd USA/Europe ATM R&D Seminar*, Napoli, Italy, June 2000.

- [2] Eurocontrol, "Performance Review Report for 2006," Eurocontrol, Brussels, Belgium, Tech. Rep. PRR2006, 2007.
- [3] J. Penner, *Aviation and the Global Atmosphere*. Intergovernmental Panel on Climate Change (IPCC): Cambridge Univ Press, 1999.
- [4] D. Black, J. Black, T. Issarayangyun, and S. Samuels, "Aircraft noise exposure and resident's stress and hypertension: A public health perspective for airport environmental management," *Journal of Air Transport Management*, vol. 13, no. 5, pp. 264–276, 2007.
- [5] A. Warren, K. Tong, B. Manage, and W. Seattle, "Development of continuous descent approach concepts for noise abatement," in *Proc. 21st AIAA/IEEE Digital Avionics Systems Conference*, vol. 1, 2002.
- [6] A. Melrose, "Basic continuous descent approach," *Airports and Environmental Management, EATM*, 2004.
- [7] F. Wubben and J. Busink, "Environmental benefits of continuous descent approaches at Schiphol Airport compared with conventional approach procedures," *National Aerospace Laboratory NLR*, no. NLR-TP-2000-275, 2000.
- [8] J. Clarke, N. Ho, L. Ren, J. Brown, K. Elmer, K. Tong, and J. Wat, "Continuous descent approach: Design and flight test for Louisville International Airport," *Journal of Aircraft*, vol. 41, no. 5, pp. 1054–1066, 2004.
- [9] Eurocontrol, "Single European Sky ATM Research Programme: SESAR," www.eurocontrol.int.sesar/public/subsitehomepage/homepage.html accessed 13/07/2010, 2005.
- [10] "Concept of operations for the next generation air transportation system ver 2.0," Joint Planning and Development Office, Washington, D.C., 2007.
- [11] H. Reynolds, T. Reynolds, and R. Hansman, "Human Factors Implications of Continuous Descent Approach Procedures for Noise Abatement in Air Traffic Control," in *Proc. 6th USA/Europe Air Traffic Management R&D Seminar, Baltimore, MD, June, 2005*.
- [12] S. Alam, H. Abbass, and M. Barlow, "Air traffic operations and management simulator ATOMS," *IEEE Transactions on Intelligent Transportation System*, vol. 9, no. 2, pp. 209–225, 2008.
- [13] P. Upham, J. Maughan, and D. Raper, *Towards Sustainable Aviation*. Earthscan, 2003.
- [14] U. Schumann, "Aircraft emissions," *Encyclopedia of Global Environmental Change*, pp. 178–186, 2002.
- [15] "Continuous Descent Approach: Implementation Guidance Information," *Environmental Unit, Eurocontrol, Brussels, Belgium*, 2007.
- [16] ICAO, *Manual of Air Traffic Services Data Link Applications*, doc 9694-an/955 ed., ICAO, Montreal, Canada, 2007.
- [17] C. Spence, Ed., *FAA Aeronautical Information Manual/Federal Aviation Regulation*. McGraw-Hill, 2003.
- [18] "User manual for base of aircrfat data (BADA)," Eurocontrol Experiment Center, Bretigny, France, Tech. Rep. Rev No:3.6, 2004.
- [19] S. Pietrzko and R. F. Hofmann, "Mathematical modelling of aircraft noise based on identified directivity patterns," in *Proc. 2nd AIAA/CEAS Aeroacoustics Conference*, no. AIAA96-1768, PA, USA, June 1996.
- [20] R. Fink, "Airframe Noise Prediction Method," Federal Aviation Administration, USA, Washington, DC, Tech. Rep. FAA-RD-77-29, 1997.
- [21] ICAO, "ICAO Engine Exhaust Emissions Databank," Montreal, Tech. Rep. Doc 9646-AN/943, 1995.
- [22] D. DuBois and G. Paynter, "Fuel Flow Method 2 for estimating aircraft emissions," *Society of Automotive Engineers Paper*, pp. 01–1987, 2006.
- [23] Sutkus, D. J. and Baughcum, S. L. and DuBois, D. P., "Commercial Aircraft Emission Scenario for 2020: Database Development and Analysis," Tech. Rep. NASA/CR-2003-212331, 2003.
- [24] Norman, P. D. and Lister, D. H. and Lecht, M. and Madden, P. and Plaisance, C. and Renger, K., "Development of the technical basis for a New Emissions Parameter covering the whole Aircraft operation: NEPAIR," Tech. Rep., 2003.
- [25] E. Zitzler, L. Thiele, M. Laumanns, C. M. Fonseca, and V. G. da Fonseca, "Performance assessment of multiobjective optimizers: An analysis and review," *IEEE Trans. on Evolutionary Computation*, vol. 7, no. 2, pp. 174–188, 2003.
- [26] H. Abbass, "The self-adaptive pareto differential evolution algorithm," in *Congress on Evolutionary Computation (CEC2002)*, vol. 1, 2002, pp. 831–836.
- [27] Air Services Australia, *Designated Airspace Handbook*, Air Services Australia, Canberra, Australia, Nov 2004.
- [28] S. Mohleji and et.al., "Curved approaches in the netherlands: feasibility and benefits," MITRE, Tech. Rep. MTR99W99W122, 1999.
- [29] A. Wennerberg and M. Gibellini, "Time Based Separation: CDG REAL-TIME SIMULATION RESULTS," EUROCONTROL Experimental Centre, Bretigny, France, Tech. Rep. EEC Note No. 17/06, 2006.

Email Addresses:

S. Alam: s.alam@adfa.edu.au
M. H. Nguyen: minha_76@yahoo.com
H. A. Abbass: h.abbass@adfa.edu.au
C. Lokan: c.lokan@adfa.edu.au
M. Ellejmi: mohamed.ellejmi@eurocontrol.int
S. Kirby: stephen.kirby@eurocontrol.int

29th IEEE/AIAA Digital Avionics Systems Conference
October 3-7, 2010